INTERFACE

royalsocietypublishing.org/journal/rsif

Research



Cite this article: He Z, Liu Z, Li M, Hui C-Y, Jagota A. 2021 Meso-scale dislocations and friction of shape-complementary soft interfaces. *J. R. Soc. Interface* **18**: 20200940. https://doi.org/10.1098/rsif.2020.0940

Received: 21 November 2020 Accepted: 12 January 2021

Subject Category:

Life Sciences-Engineering interface

Subject Areas:

biomaterials, bioengineering, biomimetics

Keywords:

dislocations, friction, soft materials, shape complementary

Author for correspondence:

Anand Jagota e-mail: anj6@lehigh.edu

Electronic supplementary material is available online at https://doi.org/10.6084/m9.figshare. c.5287632.

THE ROYAL SOCIETY

Meso-scale dislocations and friction of shape-complementary soft interfaces

Zhenping He¹, Zezhou Liu³, Meng Li^{1,4}, Chung-Yuen Hui³ and Anand Jagota^{1,2}

 1 Department of Bioengineering, and 2 Department of Chemical and Biomolecular Engineering, Lehigh University, Bethlehem, PA, USA

³Department of Mechanical and Aerospace Engineering, Cornell University, Ithaca, NY, USA
⁴College of Mechanical and Electrical Engineering, Nanjing University of Aeronautics and Astronautics, Nanjing 210016, People's Republic of China

(i) ZL, 0000-0002-3187-9025; C-YH, 0000-0001-7270-6000; AJ, 0000-0002-0779-0880

The interface between two surfaces patterned with complementary shapes such as arrays of ridge-channel structures or pillars accommodates relative misorientation and lattice mismatch by spontaneous production of dislocation arrays. Here, we show that the relative sliding of such an interface is accomplished by dislocation glide on the interfacial plane. An exception is the singular case where the lattices are perfectly matched across the sample dimension, in which case sliding is accompanied by motion of edge-nucleated defects. These are meso-scale analogues of molecular sliding friction mechanisms between crystalline interfaces. The dislocations, in addition to the long-range elastic energy associated with their Burgers vectors, also cause significant out-of-plane dilation, which props open the interface locally. For this reason, the sliding friction is strongly pressure dependent; it also depends on the relative orientation of the patterns. Sliding friction can be strongly enhanced compared with a control, showing that shape-complementary interfaces can be engineered for strongly enhanced pressure- and orientation-dependent frictional properties in soft solids.

1. Introduction

Modifying surface mechanical properties such as friction and adhesion by near-surface architecture is of great interest as a paradigm for designing unique functionality in surface mechanical properties of materials. Nature has provided many fascinating examples of surface attachment structures in biological organisms that provide unique adhesion and friction properties [1,2]. A well-known example is the class of fibrillar surface structures found in geckos [3,4], spiders [5] or some insects [6–8] which provide the ability of direction-dependent and switchable friction and adhesion [9]. Experimental and theoretical studies have revealed that the particular adhesive and frictional properties of these surfaces come from their special geometric shape design, contact splitting and high compliance [8,10–14]. Inspired by this, much scientific effort has been devoted to developing biomimetic and bioinspired structured surfaces over the last two decades, and fruitful achievements have been obtained by many research groups [2,15–17].

Although considerable progress has been made in designs of microstructures for controllable adhesion and friction, it has been mostly for one-sided surface structures, usually against a generic flat surface. In fact, all natural and almost all artificial surfaces are rough, and interesting properties are achieved when the microstructured surface in some sense matches the roughness [18,19]. Natural contacting surfaces also often exist as designed complementary pairs. Examples include the interlocking between insects' hard claws and rough substrates [20,21], the attachment structures in the dragonfly head-arresting system [22], the hydrogen bonds between two nucleotides on opposite complementary DNA or RNA [23] and the celebrated case of loop-clasp designs

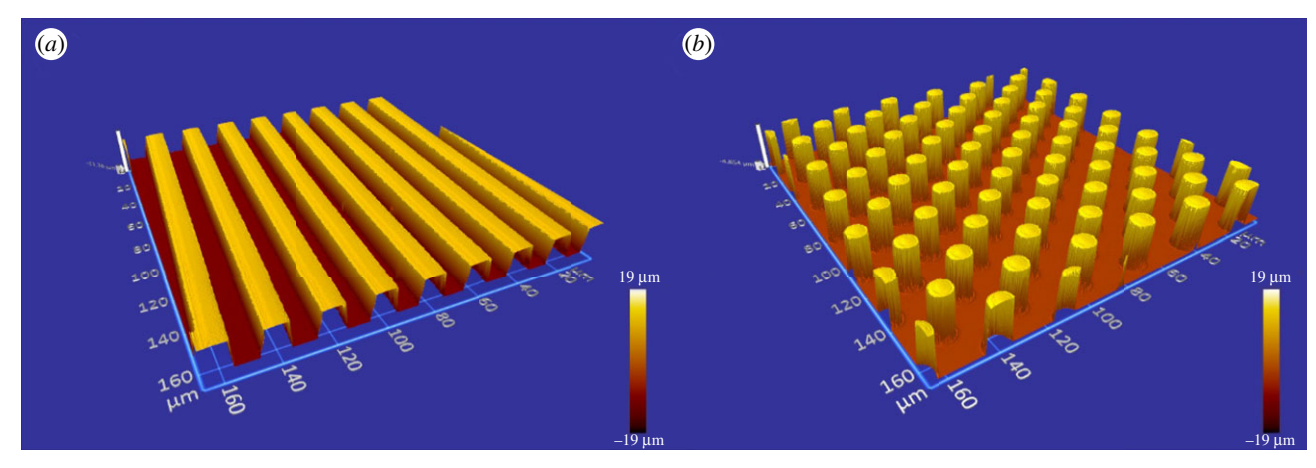


Figure 1. Three-dimensional profiles of (a) ridge—channel and (b) pillar arrays.

that led to the development of Velcro [24]. Chen et al. [25] showed how complementary fibrillar interfaces can be used to control adhesion. Guduru & Bull [26,27] showed that adhesion between a soft solid and a wavy rigid punch is strongly enhanced compared with a flat rigid punch owing to mechanical instabilities. Vajpayee et al. [28] demonstrated that shape-complementary surfaces obtained by replica moulding against rippled surfaces result in contact pairs with recognition, adhesion enhancement owing to mechanical instabilities and selectivity of adhesion, i.e. poor adhesion between mismatched surfaces. Kesari & Lew [29] also showed theoretically how a model wavy rough surface can enhance effective adhesion as a result of mechanical instabilities. Ciavarella and Papangelo [30,31] similarly studied how rough surfaces can actually enhance adhesion for soft solids. This finding is different from the general rule that rough surfaces attenuate adhesion [32-35].

Our previous studies of pairs of ridge-channel surfaces showed that for complementary shapes adhesion can be enhanced by up to a factor of 40, while for non-complementary surfaces it can be reduced by a factor of about 0.25, i.e. with selectivity of a factor of 160 [36]. Adhesion enhancement was shown to be due to a combination of crack trapping and frictional resistance to pull-out of ridges from channels. Misorientation of complementary interfaces is accommodated by line defects, appearing as visible striations, that are essentially meso-scale twist boundary screw dislocations. (Mismatch of periodic spacing results in edge dislocation arrays.) While these dislocations permit surfaces to adhere for small misorientation, they carry elastic energy, the release of which attenuates the adhesion enhancement [37]. The orientation and density of these defects can be accurately described using the geometrical analysis of Moiré patterns [38]. Thus, ridge-channel structures can be used to endow a surface with high selectivity and adhesion enhancement and strongly misorientation-dependent adhesion via the action of interfacial dislocations.

The nature of friction between shape-complementary surfaces remains to be addressed. In analogy with their adhesive properties, we here ask: How do shape-complementary structures affect the sliding friction of the interface? How do the dislocations that accommodate misorientation control sliding friction mechanisms?

We present a study of friction between two shape-complementary interfaces: ridge-channel and fibrillar. We show that, in both cases, interfacial slip is accommodated by dislocation glide. The exception is the singular case in which the surfaces are sufficiently well aligned for there to be no interfacial dislocations, in which case slip is accommodated by defects that nucleate at sample edges and sweep through the sample. In this manner, friction of shape-complementary interfaces mimics that of atomistic interfaces [39–41]. In other ways, friction is quite different, e.g. we find that it is strongly pressure dependent. (We separately considered a third case in which cylindrical fibrils on one side of the interface are complementary to cylindrical holes on the other [42]. In this system, the fibrils are embedded in their matching holes only for the first separation after moulding, subsequent to which the pillars do not easily enter their complementary holes. That is, not all shape-complementary interfaces work in the manner we study here.)

We present a detailed theoretical model for the ridgechannel structure. Modelling the core structure of the screw dislocations using the framework of fracture mechanics, we are able to explain quantitatively how friction changes with applied pressure and misorientation. The mechanics of the fibrillar interface is significantly more complicated and our discussion of the mechanisms is based on comparison with simulations of the analogous atomistic systems.

2. Experimental section

2.1. Sample fabrication

Samples with two types of shape-complementary structures, ridge-channel and fibrillar, were fabricated using a commercial poly(dimethylsiloxane)-based elastomer (PDMS; Sylgard 184; Dow Corning) following the procedure described in [36]. Briefly, we mixed the PDMS prepolymer and crosslinker in a 10:1 ratio and then poured them onto a microfabricated silicon mould, followed by curing at room temperature for 2 days before being peeled off the mould. Figure 1 shows images of two types of shape-complementary structured surfaces that are three-dimensional (3D) renditions of their profile measured via an optical profilometer (Zegage; Zygo Corporation). For the pair of ridge-channel structures, the ridge height or channel depth h is about 19 µm and their width is about 10 µm, so the periodic spacing between ridge centres, which we denote by c, is about 20 μ m. The fibrils, which are organized in a square array, have heights of about 16 μm each, diameters of 10 μm and spacing of 20 μm between closest pillar centres. Flat samples with no surface structure were also fabricated to serve as control surfaces.

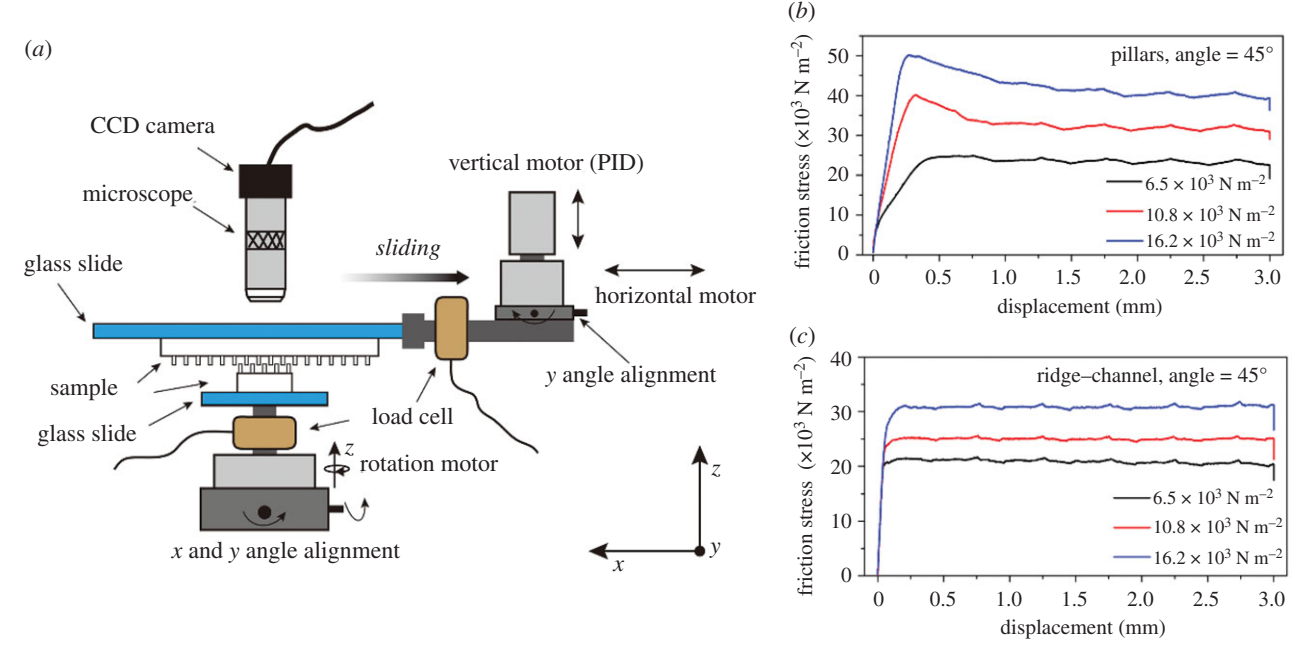


Figure 2. (a) Schematic drawing of the set-up used to measure the sliding friction of a shape-complementary interface. Representative friction versus displacement measurements for (b) a pillar–pillar square array and (c) a ridge–channel sample pair under normal stress of 6.5, 10.8 and 16.2×10^3 N m⁻², all with a misorientation angle of 45°.

2.2. Friction measurements

Friction measurements were performed using a custom-built set-up, shown schematically in figure 2a. One each of a pair of shape-complementary samples was fixed on the upper and lower glass slides by double-sided sticky tape, and the relative misorientation was precisely controlled by the rotation motor. The vertical translation motor brought the two structured surfaces in contact under force feedback control, and the horizontal motor drove the samples to slide past each other under a constant specified normal load. The lateral (friction) and normal (load) force values between the complementary surfaces were sensed by the two load cells. A LabView® program synchronized control of the motor motion, normal load feedback control and recording of forces and displacements. Before each experiment, the top and lower samples were aligned by three goniometric stages to achieve independently parallel contact between the two surfaces and alignment of the interfacial plane with the sliding axis, both to less than $1 \, \mu m$ over $3 \, mm$ of travel. The lower sample dimension was fixed to be 3.2 mm × 3.2 mm, while the upper sample was significantly larger, usually 10 mm × 10 mm. During the experiment, the top sample was moved at $5 \mu m s^{-1}$ over a distance of 3 mm under normal loads of 67-225 mN. (A full set of friction measurements were also performed under normal displacement control, which gave very similar results to those described below.) The structure of the interface and its evolution was recorded by a CCD camera attached to an optical microscope objective. Figure 2b,c shows representative friction force measurements for the two types of complementary surfaces under normal loads of 67, 111 and 166 mN with a misorientation angle of 45°.

3. Results and discussion

3.1. Interfacial structure: meso-scale dislocation arrays

Figure 3 shows optical images of the interfacial plane for ridge-channel (figure 3a-d) and fibrillar (figure 3e-h)

sample pairs for a misorientation angle, θ , in the range 0-45° under a normal stress of 10.8 kPa, captured before frictional sliding begins. As we have described previously [36-38], misorientation is accommodated by arrays of screw dislocations, as indicated in figure 3 by the blue dashed lines for ridge-channel samples and the white lines for the pillar–pillar samples. For perfect alignment, $\theta = 0^{\circ}$, there are no dislocations, and the sample is visibly uniform. Ridges are fully inserted into channels (figure 3a) and pillars (figure 3e) are in perfect synchrony, either tip on tip or tip in gaps in the complementary surface. (As soon as relative sliding begins, however, most of the tips fall into the gaps on the complementary surface.) On increasing the misorientation angle to 5°, we observe two forms of light intensity patterns on the interface. With increasing misorientation angle, the density of these patterns also increases.

As reported previously [37], for the ridge–channel pair, the dark regions are where ridges on one side of the interface are aligned with, and have entered into, channels on the other side. Lighter regions are where ridges climb over a ridge on the other side to enter the adjacent channel, which can be considered as a screw dislocation with a Burgers vector of magnitude equal to the periodic lattice spacing. For the array of fibrils, the dark regions are where the pillars from the two sides of the interface are in synchrony. These are separated by two mutually orthogonal sets of lighter strips (marked by white dashed lines in figure 3f). In these light regions, the pillars of two side interfaces are out of synchrony; these lines comprise pairs of screw dislocation arrays.

As discussed previously [38], the orientation α and density ρ of these dislocation arrays correspond to those of the Moiré patterns formed by the structures on the two surfaces. Specifically, for the ridge–channel structure

$$\alpha = \tan^{-1} \left[\frac{\sin \theta}{\lambda - \cos \theta} \right] = \pi/2 - \theta/2 \text{ (for } \lambda = 1),$$
 (3.1)

$$\rho = \frac{1}{c}\sqrt{1 + \lambda^2 - 2\lambda\cos\theta} = \frac{\sqrt{2(1 - \cos\theta)}}{c} \text{ (for } \lambda = 1), (3.2)$$

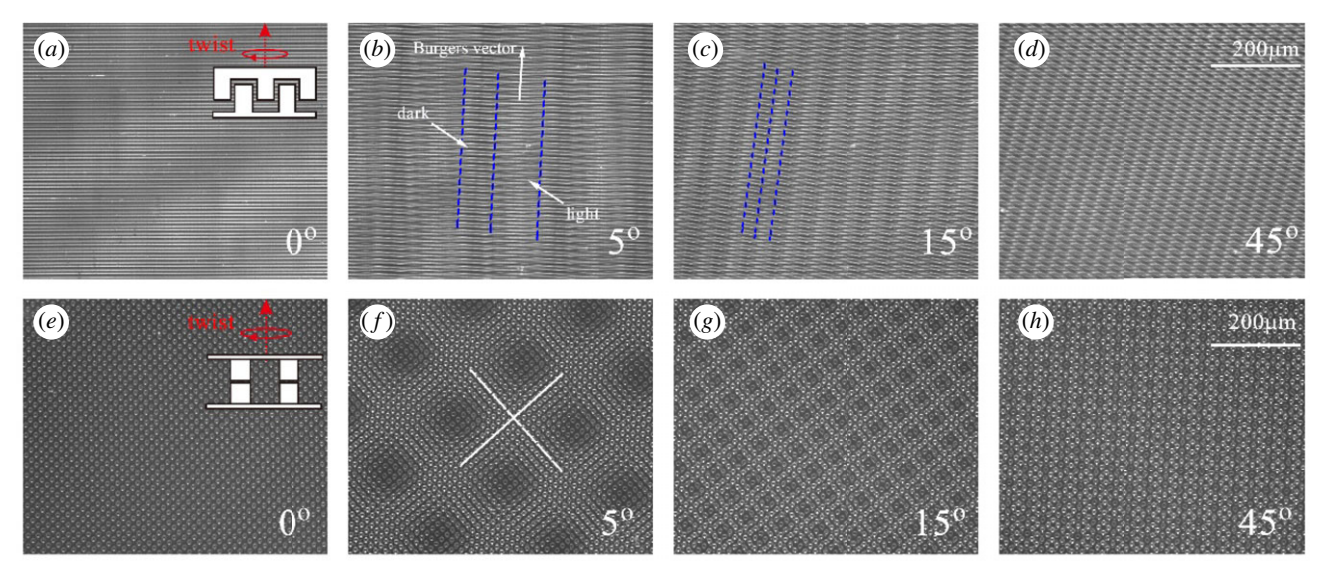


Figure 3. Optical micrographs of complementary (a-d) ridge—channel interfaces and (e-h) square array of pillars interfaces with a misorientation angle of $0-45^{\circ}$ at a load of 10.8 kPa.

where c is the periodic spacing, λ is the relative biaxial stretch between the two surface patterns (equal to unity for the experiments reported here) and θ is the misorientation angle. We can see from equation (3.1) that, for the ridge-channel structure, the orientation of the dislocation array is orthogonal to the average orientation of the ridges on the two surfaces.

3.2. Sliding friction of shape-complementary interfaces

We have previously shown that well-aligned ridge—channel interfaces result in strongly enhanced adhesion [38]. Adhesion is attenuated both by an increase in periodic spacing (Burgers vector) and by misalignment, the latter endowing the interface with additional orientation dependence of adhesion. Both these effects arise as a result of the release of energy stored in the interfacial dislocation array and can be modelled quantitatively as such. We now seek to understand the mechanisms for relative sliding of these interfaces and how the attendant frictional force depends on structure and external conditions.

3.2.1. Ridge—channel interface: observations

Figure 4a presents the results of frictional stress as a function of normal stress for the ridge-channel structure as well as a control sample. In the control sample, one of the structured surfaces is retained while the other is replaced by a flat, unstructured surface. For the control sample, friction is only weakly dependent on normal stress. The frictional stress is about 25 kPa; since only half the nominal area is in contact, the true frictional stress is about 50 kPa. The gradual increase in friction with increasing applied pressure can be explained by an increase in area of the contact owing to lateral Poisson expansion of the ridges. For well-aligned structured shape-complementary samples, the frictional stress is strongly enhanced, by up to a factor of about 6 compared with the control sample. Above a critical pressure, which increases with increasing misorientation, we observe strong dependence of friction on pressure and misorientation.

Figure 4*b* shows optical micrographs of the interface before and during sliding for a misorientation of 5°. Video RT20RT20_-82.883dg_down12_partial_compressed.mp4 in the electronic supplementary material shows how the

structure of the interface evolves during the initiation of relative sliding. It shows that, for sliding in the vertical direction, the dislocation array translates horizontally. As the pattern translates horizontally for one period, it deposits one Burgers vector (magnitude c) worth of slip in the vertical direction.

For sufficiently large misorientation, below a critical pressure, ridges do not enter the channels at all; for these cases, the friction is no greater than that of the control. Consider, for example, the case of 30° misorientation. For the two lower pressures, the ridges remain on top of the ridges of the opposing surface and friction is about the same as that of the control. For the higher four pressures, the ridges increasingly enter into the channels and friction increases significantly above that of the control. Figure 4c shows a magnified view of the dislocation structure during sliding, where we also sketch a diagram of the cross-section of an interface. It indicates that, during sliding, a ridge has to switch sides with its equivalent ridge on the opposite surface. This necessarily requires an intermediate state in which the dislocation core is dilated.

The foregoing discussion suggests that the dislocation core can be treated as a crack under mixed-mode loading, and that the misorientation and load dependence of friction can perhaps both be explained in terms of partially opened cracks near the dislocation core. This idea is further developed below, generalizing our previous approach to this problem in which we accounted for the mode III component (screw dislocation) but not for dilation or external pressure and shear loading [37,38].

3.2.2. Model for friction of a complementary ridge—channel interface

It is instructive to compare the screw dislocation described above with the Volterra screw dislocations in the continuum theory [43,44]. The structure of the screw dislocations of our experiments is shown schematically in figure 4d and a magnified view of the dislocation core is presented in figure 4e. At the interface, ridges (white) of the top sample (blue) rise out of their complementary channels, cross over the ridges of the other surface (shaded) of the bottom sample (green) and enter into the adjacent channels. The regions where ridges fail to fully insert into channels are the dislocation

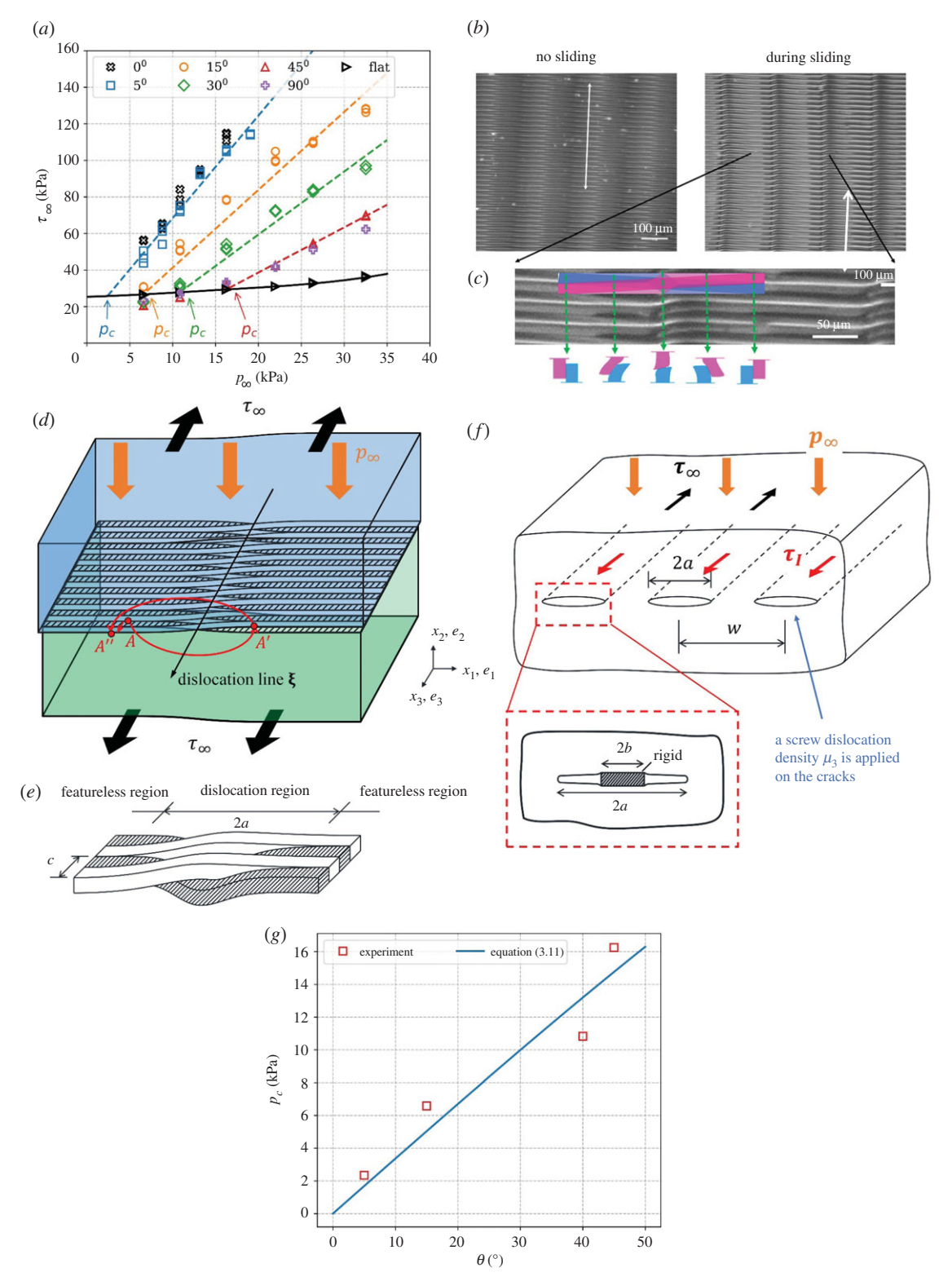


Figure 4. (a) Friction stress versus applied pressure for the ridge—channel sample pair with different misorientation angles (experimental data are represented by symbols), (b) optical micrographs of the ridge—channel complementary interface captured before/during sliding at the misorientation of 5° , (c) the deformation of the interlocked ridge—channel pair at the misorientation of 5° during sliding and (d) schematics of the screw dislocation array subject to external and internal forces. Along the interface between the two samples, ridges rise out of their complementary channels and enter into the adjacent channels. The dislocation line is in the x_3 direction. The applied normal pressure and shear stress are indicated by the orange and black arrows, respectively. (e) Schematic of the dislocation core. (f) Schematic of the analytical model for friction of a complementary ridge—channel interface. (g) Comparison of the critical pressures predicted by equation (3.11) with those observed in experiments.

cores; each core occupies a width of 2a [37]. The regions where ridges are completely inserted into channels appear featureless in optical micrographs. From the viewpoint of the Volterra theory, the size of the ridges and channels would be taken to be sufficiently small so that they could be neglected in the analysis. In addition, the core size 2a

would be taken to be zero, resulting in a singular stress field. The dislocation line lies in the x_3 direction. The Burgers vector is the sudden jump in displacement as one moves along a circuit (Burgers circuit) that encloses the dislocation core and, for a screw dislocation, it is parallel to the dislocation line. Specifically, as depicted in figure 4d, the Burgers

vector can be obtained by moving from point A to point A' in the bottom sample (green), and from point A' to point A'' in the top sample (blue). It is evident that the Burgers vector is $B = \overrightarrow{A''A} = ce_3$.

In the continuum theory, when a screw dislocation is subjected to a shear stress τ_{∞} and normal pressure p_{∞} , the energetic force (or Peach–Koehler force $F_{\rm PK}$) acting on the dislocation is given by [43,45]

$$F_{\rm PK} = (\sigma \cdot B) \times \xi, \tag{3.3}$$

where σ is the remote stress field, B is the Burgers vector and ξ is a unit vector along the dislocation direction. Taking $B=ce_3,~\xi=e_3$ and $\sigma=-\tau_\infty e_2\otimes e_3-\tau_\infty e_3\otimes e_2-p_\infty e_2\otimes e_2$, the Peach–Koehler force is

$$F_{\rm PK} = -\tau_{\infty} e_1. \tag{3.4}$$

Note that F_{PK} is in the negative x_1 direction, which is perpendicular to the direction of the applied shear. This is consistent with the experimental observations that vertical relative sliding is accommodated by horizontal glide of the dislocation (see videos in the electronic supplementary material). However, according to (3.4), the Peach-Koehler force, F_{PK} , for a screw dislocation is independent of the normal pressure—this contradicts the observations (figure 4a). Additionally, the dislocations are typically modelled as line defects, ignoring the structure of the core, and the results are independent of structural parameters such as the ridge height or width. In previous work, we have shown how adhesion can be adequately modelled based on classical dislocation theory [37,38]. However, since normal pressure and details of the core structure have a significant impact on friction, the classical Volterra theory alone cannot adequately address how these control friction. To understand how friction depends on the applied pressure and misorientation, it is, therefore, necessary to study the interaction of the dislocation core with the applied pressure and shear, and this is what we will do next.

Our approach to model such a structure is to treat these dislocation cores as mode I and mode III periodic cracks of width 2a, wedged open by the dilation due to the ridges crossing on top of each other (mode I), under applied normal pressure p_{∞} (mode I) and applied shear stress τ_{∞} (mode III). To account for the screw dislocation, a screw dislocation density μ_3 is applied on the cracks (mode III). μ_3 is unknown and should be determined by the boundary conditions. In addition, one expects considerable resistance to deformation by the dislocation cores where the ridges cross; for example, bending and torsion of ridges and frictional stress on the contacting interfaces. For simplification, we replace such complicated resistance to the motion of the screw dislocation by an internal shear stress $\tau_{\rm I}$ on the crack faces (mode III), as shown in figure 4f. Note that $\tau_{\rm I}$ could depend on the local deformation, stress state, contact area and surface architecture. These cracks are infinitely long in the x₃ direction. The spacing between crack centres or period is denoted by w. Equation (3.2) is equivalent to

$$w = \frac{c}{2\sin\left(\theta/2\right)}. (3.5)$$

The mode III stress intensity factors $K_{\rm III}^{(1)}$ due to the screw dislocation density μ_3 can be found as (derivation is provided

in the electronic supplementary material)

$$K_{\text{III}}^{(1)} = \frac{Gc}{2\sqrt{w\tan(\pi a/w)}}.$$
 (3.6a)

The mode III intensity factors at each crack tip due to the applied shear stress τ_{∞} and the internal shear stress $\tau_{\rm I}$ are simply given by *The Stress Analysis of Cracks Handbook* [46],

$$K_{\rm III}^{(2)} = \tau_{\infty} \sqrt{w \tan \frac{\pi a}{w}} \,, \tag{3.6b}$$

$$K_{\rm III}^{(3)} = \tau_{\rm I} \sqrt{w \tan \frac{\pi a}{w}}. \tag{3.6c}$$

The stress intensity factor of the mode I model at the crack tip is approximately given by The Stress Analysis of Cracks Handbook [46],

$$K_{\rm I} = [E^*h/2 - p_{\infty}a(K(k) - E(k))]\frac{1}{kK(k)}\sqrt{\frac{\pi}{a}},$$
 (3.7a)

where E^* is the plane-strain Young's modulus, $k = \sqrt{1 - (b/a)^2}$ (2b is the wedge width; figure 4f), h is the wedge opening displacement (i.e. ridge height) and K(k) and E(k) are complete elliptic integrals of the first and second kind, respectively. The first term in the square bracket represents crack opening due to the dilation, and the second term implies crack closure due to the applied pressure. However, this model overestimates K_I since it assumes that the wedge is rigid at the crossovers. Thus, to compensate the compliance of ridges at the crossovers, we replace E*h/2 with a fitting parameter P_I in (3.7a), i.e.

$$K_{\rm I} = [P_{\rm I} - p_{\infty} a(K(k) - E(k))] \frac{1}{kK(k)} \sqrt{\frac{\pi}{a}}$$
 (3.7b)

How to determine P_1 will be discussed later. The energy release rate, which is denoted by Γ , is

$$\Gamma = \frac{K_{\rm I}^2}{E^*} + \frac{K_{\rm III}^2}{2G}$$
, where $K_{\rm III} = K_{\rm III}^{(1)} + K_{\rm III}^{(2)} + K_{\rm III}^{(3)}$. (3.8)

The condition for quasi-static sliding is that the applied energy release rate should equal the work of adhesion

$$\Gamma = W_{\rm ad}$$
, (3.9)

where $W_{\rm ad}$ is the work of adhesion. Note that this condition is applied at the opening end of the crack that represents the dislocation core. At the closing end of the crack, there is no energy release rate. While in the far field we have a screw dislocation with a well-defined Burgers vector, in the near field we have a dislocation core that propagates following a fracture criterion, instead of the usual singularity at the core of a Volterra dislocation. In one dimension, the ridge smoothly goes from one channel to the other and there are no special instabilities.

We now turn to the experiments. Using our model, we first explain the observation that, when the applied pressure p_{∞} is greater than a critical value p_c , the applied shear stress is significantly above that of the control. The values of p_c can be obtained graphically in figure 4a—they are either the last data points remaining on the control curve (black line) as one increases the applied pressure or the intersection of the control curve (black line) and the extrapolation of the points above the control (dashed lines). Physically, $p_{\infty} = p_c$ is the pressure above which the near-surface structures start to insert into each other. If $p_{\infty} < p_c$, the ridges remain on top

of the ridges of the opposing surface so that the applied shear stress τ_{∞} is about the same as the control. We assume that the energy release rate $K_{\rm I}$ owing to mode I is zero (or negligible) at $p_{\infty}=p_c$. This assumption is consistent with Jin *et al.* [37] and Dillen *et al.* [38], who demonstrated that the energy release rate owing to dilation is negligibly small under no applied pressure, and the applied pressure would further reduce the value of $K_{\rm I}$. Setting (3.7b) to zero, the critical pressure p_c is

$$p_c = \frac{P_{\rm I}}{a[K(k) - E(k)]}. (3.10)$$

To fit the data, based on experimental observation, we set the ratio b/a to be 0.2. The crack length 2a is an unknown, albeit bounded by w. However, from figure 3, it appears that a decreases rapidly with increasing misorientation angles θ , and is equal to 0.25–0.3w. We set $a=0.3w=0.15c/\sin{(\theta/2)}$ in the following calculations. Thus, the critical p_c in our sliding system is

$$p_c \approx 38.56 \sin \left(\theta/2\right) \text{ kPa},$$
 (3.11)

with the fitting parameter $P_{\rm I} = 268.5 \text{ mN m}^{-1}$. We plot the critical pressure p_c predicted by our model in figure 4g. It shows good agreement with the experimental data (squares).

Next, we complete our analysis by providing an approximate formula for the $p_{\infty} - \tau_{\infty}$ relation at different misorientations. As mentioned, the contribution from mode I is small as long as $p_{\infty} > p_c$, thus the quasi-static condition for sliding becomes

$$\frac{\left[K_{\text{III}}^{(1)} + K_{\text{III}}^{(2)} - K_{\text{III}}^{(3)}\right]^{2}}{2G} = W_{\text{ad}}, \text{ for } p_{\infty} > p_{c}.$$
(3.12)

As the sliding system is found to be pressure sensitive, we assume that $\tau_{\rm I}$ is linearly related to the applied pressure p_{∞} (i.e. a first-order approximation),

$$\tau_{\rm I} = \alpha p_{\infty} + \beta, \tag{3.13}$$

where α and β are the friction coefficients. α and β can depend on the work of adhesion, pressure and misorientation. Substituting (3.6*a*–3.6*c*) and (3.13) into (3.12) leads to

$$\tau_{\infty} = \alpha p_{\infty} + \beta + \frac{\sqrt{2GW_{\rm ad}}}{\sqrt{w \tan{(\pi a/w)}}} - \frac{Gc}{2w \tan{(\pi a/w)}}. \quad (3.14)$$

Therefore, the following formula can be used to predict the applied shear stress for $5^{\circ} \le \theta \le 45^{\circ}$:

$$\tau_{\infty} = \begin{cases} \alpha p_{\infty} + \beta + \frac{\sqrt{2GW_{ad}}}{\sqrt{w \tan{(\pi a/w)}}} - \frac{Gc}{2w \tan{(\pi a/w)}} & p_{\infty} \ge p_c, \\ f^{\text{control}}(p_{\infty}) & p_{\infty} < p_c, \end{cases}$$

$$(3.15)$$

where f^{control} is the friction stress of the control sample. The work of adhesion, W_{ad} , of the structure is also an unknown. It was reported by Dillen et~al. [38] that the work of adhesion for a flat interface is of the order of 0.075 J m⁻², and this value can be enhanced by up to tens of times for a shape-complementary ridge–channel interface. For simplification, we assume that the work of adhesion is a constant and independent of pressure and misorientation. We take $W_{\text{ad}} = 0.1 \text{ J m}^{-2}$. Using the experimental data and enforcing that (3.15) must pass through the point (p_c , $f^{\text{control}}(p_c)$), we can fit α and β (values are given in the electronic supplementary material) and then use (3.15) to predict τ_{∞} as represented

by the dashed lines in figure 4a. Our predictions and the experimental data agree very well.

3.2.3. Fibrillar interface

Figure 5a presents the measured sliding frictional stress for a fibrillar shape-complementary interface as a function of normal stress for a few different misorientation angles. As a control, the friction of a fibrillar surface sliding against a flat sample is also included. For normal pressure p_{∞} less than about 16 kPa, the control sample has an approximately pressure-independent sliding friction of about 10 kPa. (Accounting for the actual area of contact, the sliding stress is approx. 50 kPa, about the same value as in the ridge-channel geometry, unsurprisingly.) A pressure-independent sliding frictional stress for smooth contacts is consistent with previous measurements on PDMS [47,48]. However, between 16 and 20 kPa, the sliding friction of the control increases rapidly. Examination of the contact region reveals that this transition corresponds to buckling of the fibrils such that their lateral sides come into contact, significantly increasing the area of contact, a phenomenon that has been reported previously [48]. (See also electronic supplementary material, video FibrilFC_Rt20fc_Down60_Partial-1_s.mp4 for an example of a control experiment under normal stress below the transition.)

The frictional stress of the fibril–fibril interface is strongly enhanced, again by a factor of up to 6, compared with the (unbuckled) control. In contrast with the intrinsic friction between the PDMS surfaces, the structured interface has strongly pressure-dependent friction. The highest shear stress is observed at perfect alignment and the shear stress generally drops as misalignment increases. However, the attenuation of friction due to misorientation is much milder than in the ridge–channel case. We propose that the weak misorientation dependence is because, in the pillar–pillar case, the interfacial arrangement changes periodically every 45° and because the fibrils can bend nearly independently.

Figure 5c shows a comparison of two optical images of the interface for a misorientation angle of 5° before and during sliding. The image of the interface before sliding shows, as mentioned previously, two regions. In the dark region, fibrils on the two surfaces are aligned. In analogy with twist grain boundaries, the orientation and density of this pattern is given by the geometry of the corresponding Moiré pattern [38,49]. Also in analogy with twist grain boundaries, the interface splits into two regions [50,51], in which the fibrils on the two surfaces are aligned with each other. These are separated by lighter regions that contain arrays of screw dislocations.

Electronic supplementary material, video Rt20Rt20_5dg_down12_s.mp4 shows how the pattern just described (prior to sliding) evolves under applied shear (relative sliding in the vertical direction). The first observation is that sliding in the vertical direction is accompanied by motion of the pattern in the horizontal direction. This is for the same reason as discussed for the ridge—channel structure. While the pattern retains its overall density and orientation, it acquires directionality, losing symmetry in the horizontal direction. Recognizing pattern translation as equivalent to dislocation motion, it is evident that sliding is accommodated by dislocation glide on the interfacial plane. Translation of the pattern by one period corresponds to vertical sliding by c, depositing a Burgers vector worth of shear at the sample edges. It is also consistent

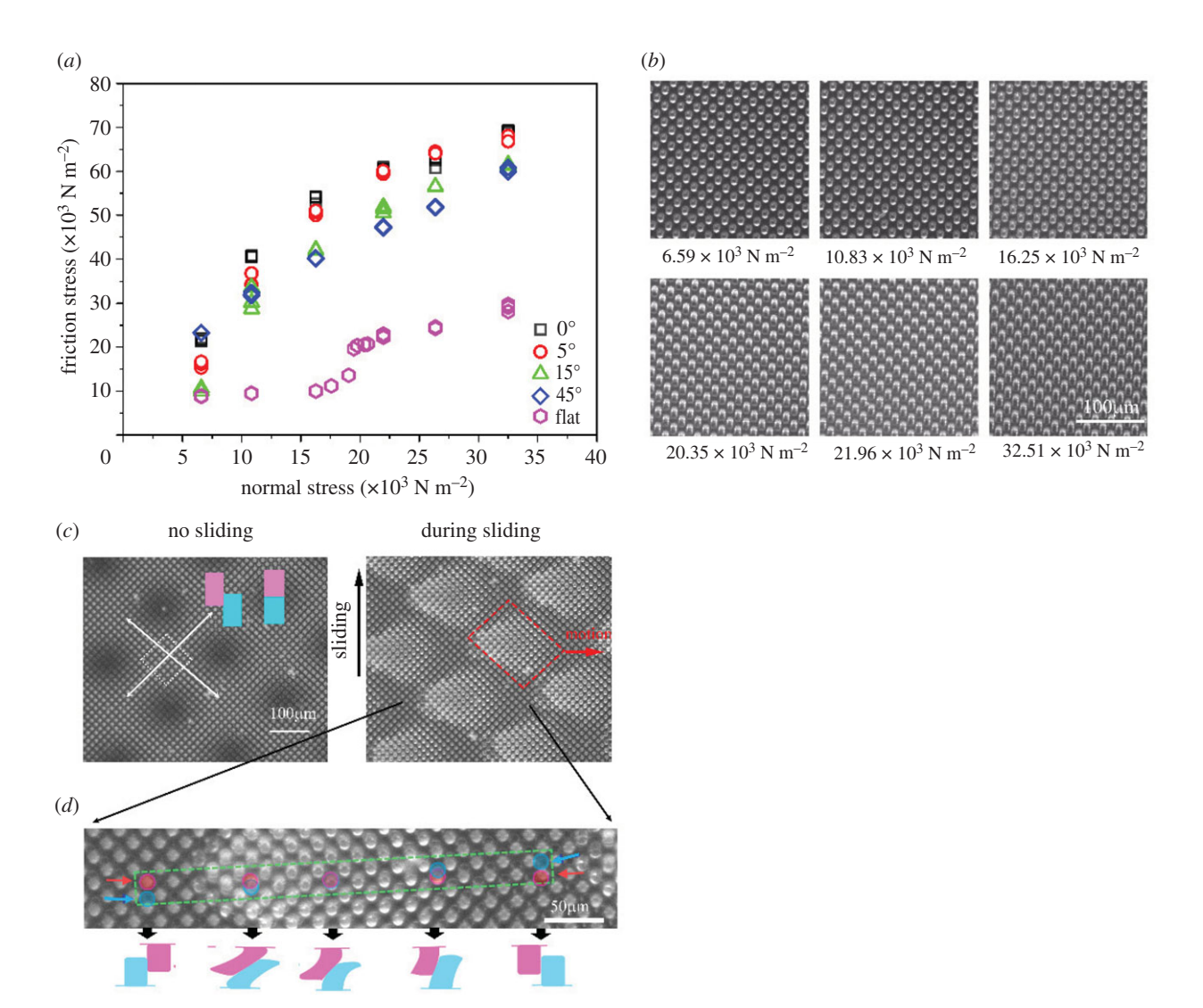


Figure 5. (a) Frictional stress versus normal stress for the square fibrillar sample pair with different misorientation angles compared with a control. The shape-complementary interface has strongly enhanced and normal-pressure-dependent friction. (b) Optical micrographs of the contact region of pillars sliding against a flat control with varying normal stress and (c) the shape-complementary interface captured before/during sliding at the misorientation of 5° . (d) Because the patterns translate horizontally for a single period for sliding vertically by one Burgers vector, the spatial horizontal variation can be viewed as the time history of a single fibril.

with the direction of the Peach–Koehler force. Thus, we see that the structure and kinematics of sliding can be understood in terms of dislocation structures.

We turn now to a discussion of sliding friction stress, starting with a closer examination of the deformation in figure 5d. Because the pattern translates by one period in the horizontal direction for one Burgers vector worth of sliding in the vertical direction, the spatial variation depicted in figure 4d is identical to the temporal variation of a given fibril. Follow the deformation of two fibrils (coloured blue and pink, one on each surface) from right to left. The pair begin in a state in which the blue fibril is trapped in a gap made by four fibrils on the other side. As we move to the left, the blue and pink fibrils impinge on each other to accommodate relative sliding. This is accompanied by dilation of the interface in the out-ofplane direction. At a critical condition, the fibrils slide past each other, now entering a gap adjacent to the original one. The drawings below the micrograph in figure 4d depict this sequence of events. Clearly, the force resisting and abetting pillar motion is periodic and is in this sense analogous to inter-atom potentials for pairs of atoms on two sides of an interface. In fact, sliding accommodated by interfacial dislocation glide is similar to that found in atomistic simulation [39]. The detailed analysis of the dislocation core structure in the fibrillar case is considerably more complicated and is the subject of future work.

4. Summary and conclusion

Interfaces between soft solids with ordered shape-complementary surface features accommodate misorientation by spontaneous formation of meso-scale dislocations. The density and orientation of the dislocation arrays depend on misorientation and orientation of the Burgers vector. In this work, we studied how sliding friction of such an interface depends on the material's parameters, geometry and external influences such as applied pressure and misorientation. We carried out a series of controlled friction tests on two shape-complementary interfaces: ridge-channel and fibrillar, with varying pressure, while progressively increasing the misalignment angle. In both cases, we found that although friction of control samples is low and relatively independent of pressure, that of shape-complementary interfaces is strongly pressure dependent and significantly enhanced compared with the control for well-aligned samples. Sliding of the interface is accommodated by dislocation glide in a

direction orthogonal to sliding. In many ways, these mesoscale dislocations mimic those in crystalline solids at the atomic scale. However, in other ways they do not, specifically in their strong sensitivity to applied pressure. For the ridgechannel case, treating the dislocation core as a crack under internal and external mixed-mode loading, we developed a model that accurately captures experimental measurements. Although the defects are well described as arrays of screw dislocations, the core structure is very different from that found in atomic systems. By representing the dislocation core as a crack, we have postulated a criterion for sliding based on external and internal forces providing sufficient stress intensity for the crack to propagate. For the fibrillar system, our observations are of a similar nature. However, the system is a closer mimic of atomistic interfaces and it may be possible to apply methods developed in that field [52]; we leave this more complicated quantitative model for future work. In this work, our focus has been on elastic materials and thus the criterion for quasi-static sliding, equation (3.9), has no dependence on rate. Phenomenologically, one could build in a rate effect by allowing work of adhesion to depend on velocity, so that the sliding condition of equation (3.9) becomes $\Gamma = W_{\rm ad}(v)$. This could be adequate for handling near-interface rate effects. However, coupling of the (elastic) structure effects studied in this work with bulk viscoelasticity would be a much bigger undertaking.

Our work shows that shape-complementarity can be used to endow interfaces between generic materials with selectivity of adhesion and friction, and orientation/pressure-controlled friction.

Data accessibility. Most of the data have been presented in figures in the main text. We have also included four videos in the electronic supplementary material.

Authors' contributions. Z.H. built the experimental set-up, conducted the first full set of experiments, interpreted data and co-wrote the manuscript. Z.L. developed the theoretical model, created several of the figures and co-wrote the manuscript. M.L. carried out all the experiments under force control and co-wrote the manuscript. C.-Y.H. co-developed the theoretical model, co-wrote the manuscript and designed research. A.J. designed research, interpreted data, contributed to the theoretical model and co-wrote the manuscript. Competing interests. We declare we have no competing interests.

Funding. This work was supported by the National Science Foundation, through a LEAP-HI/GOALI grant, CMMI-1854572. We acknowledge support for M.L. from the China Scholarship Council (grant no. 201806830076).

References

- Bhushan B. 2009 Biomimetics: lessons from nature—an overview. *Phil. Trans. R. Soc. A* 367, 1445–1486. (doi:10.1098/rsta.2009.0011)
- 2. Jagota A, Hui C-Y. 2011 Adhesion, friction, and compliance of bio-mimetic and bio-inspired structured interfaces. *Mater. Sci. Eng. R Rep.* **72**, 253–292. (doi:10.1016/j.mser.2011.08.001)
- Autumn K, Liang YA, Hsieh ST, Zesch W, Chan WP, Kenny TW, Fearing R, Full RJ. 2000 Adhesive force of a single gecko foot-hair. *Nature* 405, 681–685. (doi:10.1038/35015073)
- Autumn K, Peattie AM. 2002 Mechanisms of adhesion in Geckos1. *Integr. Comp. Biol.* 42, 1081–1090. (doi:10.1093/icb/42.6.1081)
- Kesel AB. 2003 Adhesion measurements on the attachment devices of the jumping spider *Evarcha* arcuata. J. Exp. Biol. 206, 2733–2738. (doi:10.1242/ jeb.00478)
- Eisner T, Aneshansley DJ. 2000 Defense by foot adhesion in a beetle (*Hemisphaerota cyanea*). *Proc. Natl Acad. Sci. USA* 97, 6568–6573. (doi:10.1073/ pnas.97.12.6568)
- Gorb SN et al. 2002 Structural design and biomechanics of friction-based releasable attachment devices in insects. Integr. Comp. Biol. 42, 1127–1139. (doi:10.1093/icb/42.6.1127)
- 8. Arzt E, Gorb S, Spolenak R. 2003 From micro to nano contacts in biological attachment devices. *Proc. Natl Acad. Sci. USA* **100**, 10 603–10 606. (doi:10.1073/pnas.1534701100)
- Scherge M, Gorb SN. 2001 Biological micro- and nanotribology. Berlin, Germany: Springer Science & Business Media.
- 10. del Campo A, Greiner C, Arzt E. 2007 Contact shape controls adhesion of bioinspired fibrillar surfaces.

- *Langmuir* **23**, 10 235—10 243. (doi:10.1021/la7010502)
- Bartlett MD, Croll AB, King DR, Paret BM, Irschick DJ, Crosby AJ. 2012 Looking beyond fibrillar features to scale gecko-like adhesion. *Adv. Mater.* 24, 1078–1083. (doi:10.1002/adma. 201104191)
- King DR, Bartlett MD, Gilman CA, Irschick DJ, Crosby AJ. 2014 Creating gecko-like adhesives for 'real world' surfaces. *Adv. Mater.* 26, 4345–4351. (doi:10.1002/adma.201306259)
- Gao H, Wang X, Yao H, Gorb S, Arzt E. 2005 Mechanics of hierarchical adhesion structures of geckos. *Mech. Mater.* 37, 275–285. (doi:10.1016/j. mechmat.2004.03.008)
- Glassmaker NJ, Jagota A, Hui C-Y, Noderer WL, Chaudhury MK. 2007 Biologically inspired crack trapping for enhanced adhesion. *Proc. Natl Acad.* Sci. USA 104, 10 786–10 791. (doi:10.1073/pnas. 0703762104)
- Kamperman M, Kroner E, del Campo A, McMeeking RM, Arzt E. 2010 Functional adhesive surfaces with 'gecko' effect: the concept of contact splitting. *Adv. Eng. Mater.* 12, 335–348. (doi:10.1002/adem. 201000104)
- Hensel R, Moh K, Arzt E. 2018 Engineering micropatterned dry adhesives: from contact theory to handling applications. *Adv. Funct. Mater.* 28, 1800865. (doi:10.1002/adfm.201800865)
- Kim S, Sitti M. 2006 Biologically inspired polymer microfibers with spatulate tips as repeatable fibrillar adhesives. *Appl. Phys. Lett.* 89, 261911. (doi:10. 1063/1.2424442)
- Huber G, Gorb S, Hosoda N, Spolenak R, Arzt E.
 2007 Influence of surface roughness on gecko

- adhesion. *Acta Biomater.* **3**, 607–610. (doi:10.1016/j.actbio.2007.01.007)
- Bai Y, Hui C-Y, Levrard B, Jagota A. 2015
 Enhancement of friction against a rough surface by a ridge—channel surface microstructure. *Langmuir* 31, 7581–7589. (doi:10.1021/la503838e)
- Gorb SN. 2008 Biological attachment devices: exploring nature's diversity for biomimetics. *Phil. Trans. R. Soc. A* 366, 1557–1574. (doi:10.1098/rsta. 2007.2172)
- Dai Z, Gorb SN, Schwarz U. 2002 Roughnessdependent friction force of the tarsal claw system in the beetle *Pachnoda marginata* (Coleoptera, Scarabaeidae). *J. Exp. Biol.* 205, 2479–2488.
- Gorb SN. 1999 Evolution of the dragonfly headarresting system. *Proc. R. Soc. Lond. B* 266, 525–535. (doi:10.1098/rspb.1999.0668)
- Alberts B, Johnson A, Walter P, Lewis J, Raff M, Roberts K. 2008 Molecular cell biology. New York, NY: Garland Science.
- 24. De MG. 1955 Velvet type fabric and method of producing same. US Patent no. 2,717,437.
- Chen C-M, Chiang C-L, Lai C-L, Xie T, Yang S. 2013 Buckling-based strong dry adhesives via interlocking. *Adv. Funct. Mater.* 23, 3813–3823. (doi:10.1002/adfm.201300052)
- Guduru PR. 2007 Detachment of a rigid solid from an elastic wavy surface: theory. *J. Mech. Phys. Solids* 55, 445–472. (doi:10.1016/j.jmps.2006.09.004)
- Guduru PR, Bull C. 2007 Detachment of a rigid solid from an elastic wavy surface: experiments. *J. Mech. Phys. Solids* 55, 473–488. (doi:10.1016/j.jmps.2006. 09.007)
- 28. Vajpayee S, Khare K, Yang S, Hui C-Y, Jagota A. 2011 Adhesion selectivity using rippled surfaces.

- *Adv. Funct. Mater.* **21**, 547–555. (doi:10.1002/adfm. 201001652)
- Kesari H, Lew AJ. 2011 Effective macroscopic adhesive contact behavior induced by small surface roughness. J. Mech. Phys. Solids 59, 2488–2510. (doi:10.1016/j.jmps.2011.07.009)
- Ciavarella M. 2016 On roughness-induced adhesion enhancement. J. Strain Anal. Eng. Des. 51, 473–481. (doi:10.1177/0309324716653003)
- Papangelo A, Ciavarella M. 2020 A numerical study on roughness-induced adhesion enhancement in a sphere with an axisymmetric sinusoidal waviness using Lennard-Jones interaction law. *Lubricants* 8, 90. (doi:10.3390/lubricants8090090)
- 32. Persson BNJ, Tosatti E. 2001 The effect of surface roughness on the adhesion of elastic solids. *J. Chem. Phys.* **115**, 5597–5610. (doi:10.1063/1. 1398300)
- 33. Bhushan B. 1998 Contact mechanics of rough surfaces in tribology: multiple asperity contact. *Tribol. Lett.* **4**, 1–35. (doi:10.1023/A:10191 86601445)
- 34. Greenwood JA, Williamson JBP, Bowden FP. 1966 Contact of nominally flat surfaces. *Proc. R. Soc. Lond. A* **295**, 300–319. (doi:10.1098/rspa.1966.0242)
- Fuller KNG, Tabor D. 1975 The effect of surface roughness on the adhesion of elastic solids. *Proc. R. Soc. Lond. A* 345, 327–342. (doi:10.1098/ rspa.1975.0138)
- 36. Singh AK, Bai Y, Nadermann N, Jagota A, Hui C-Y. 2012 Adhesion of microchannel-based

- complementary surfaces. *Langmuir* **28**, 4213–4222. (doi:10.1021/la204519w)
- Jin C, Jagota A, Hui C-Y. 2013 Microstructures: structure and energetics of dislocations at microstructured complementary interfaces govern adhesion. Adv. Funct. Mater. 23, 3452–3452. (doi:10.1002/ adfm.201370137)
- 38. Dillen J, He Z, Hui C-Y, Jagota A. 2016 Geometry of defects at shape-complementary soft interfaces. *Extreme Mech. Lett.* **9**, 74–83. (doi:10.1016/j.eml. 2016.05.006)
- Sharp TA, Pastewka L, Robbins MO. 2016 Elasticity limits structural superlubricity in large contacts. *Phys. Rev. B* 93, 121402. (doi:10.1103/PhysRevB.93. 121402)
- Sharp TA, Pastewka L, Lignères VL, Robbins MO.
 2017 Scale- and load-dependent friction in commensurate sphere-on-flat contacts. *Phys. Rev. B* 96, 155436. (doi:10.1103/PhysRevB.96.155436)
- 41. Manini N, Mistura G, Paolicelli G, Tosatti E, Vanossi A. 2017 Current trends in the physics of nanoscale friction. *Adv. Phys. X* **2**, 569–590. (doi:10.1080/23746149.2017.1330123)
- Paretkar D, Malhotra P, Hui C-Y, Jagota A. 2017
 Adhesion enhancement of a gel-elastomer interface by shape complementarity. In Bio-inspired structured adhesives: biological prototypes, fabrication, tribological properties, contact mechanics, and novel concepts (eds L Heepe, L Xue, SN Gorb), pp. 291–301. Cham, Switzerland: Springer International Publishing.

- 43. Hirth JP, Lothe J, Mura T. 1983 Theory of dislocations (2nd ed.). *J. Appl. Mech.* **50**, 476–477. (doi:10.1115/1.3167075)
- Volterra V. 1907 On the equilibrium of multiplyconnected elastic bodies. *Ann. Sci. Ec. Norm. Super* 24, 401–517.
- Peach M, Koehler JS. 1950 The forces exerted on dislocations and the stress fields produced by them. *Phys. Rev.* 80, 436–439. (doi:10.1103/PhysRev.80.436)
- Tada H, Paris PC, Irwin GR, Tada H. 2000 The stress analysis of cracks handbook. New York, NY: ASME Press.
- 47. Chateauminois A, Fretigny C. 2008 Local friction at a sliding interface between an elastomer and a rigid spherical probe. *Eur. Phys. J. E* **27**, 221. (doi:10. 1140/epje/i2008-10376-5)
- 48. Shen L, Jagota A, Hui C-Y. 2009 Mechanism of sliding friction on a film-terminated fibrillar interface. Langmuir 25, 2772–2780. (doi:10.1021/la803390x)
- Bollmann W. 2012 Crystal defects and crystalline interfaces. Berlin, Germany: Springer Science & Business Media.
- 50. Sutton AP, Balluffi RW. 1995 *Interfaces in crystalline materials*. Oxford, UK: Oxford Science Publications.
- Pochet P, McGuigan BC, Coraux J, Johnson HT. 2017 Toward moiré engineering in 2D materials via dislocation theory. *Appl. Mater. Today* 9, 240–250. (doi:10.1016/j.apmt.2017.07.007)
- Gao Y. 2010 A Peierls perspective on mechanisms of atomic friction. *J. Mech. Phys. Solids* 58, 2023–2032. (doi:10.1016/j.jmps.2010.09.014)